Arabian Journal of Geosciences (2018) 11: 184
https://doi.org/10.1007/s12517-018-3507-5

ICAGE 2016

Evaporation, shrinkage and intrinsic permeability of unsaturated clayey soil: analytical modelling versus experimental data

Houcem Trabelsi [1,2] · Bilel Hadrich [3] · Houda Guiras [1,4]

Received: 13 April 2017 / Accepted: 27 March 2018 / Published online: 21 April 2018

Abstract

This paper presents the experimental study conducted on a clayey soil originating from the region of Béja, north-west of Tunisia. The evaporation, shrinkage and permeability behaviours were studied. The Soil Water Retention Curve (SWRC) was determined from the slurry state to dry state, under the desiccation path (called initial drying curve). The Crack Intensity Factor (CIF), settlement and void ratio were also studied to characterise the shrinkage phenomenon during desiccation. Moisture content (ω), saturation degree (S_r) and evaporation rate (R_e) evolutions during desiccation path were also presented. This type of slurry clay presents three stages during the desiccation process (pendular, funicular and capillary regimes). During desiccation process, the evaporation rate presents a linear relationship as a saturation degree function. Furthermore, the evaporation rate versus suction presents two phases: quasi-saturated and unsaturated states. This paper introduces a study of the hygroscopic and mechanical parameters naturally modified during a desiccation process and proposes some analytical models to describe clay behaviour. Using these parameters, we can determine the intrinsic permeability during the desiccation process.

Keywords Clay · Evaporation · Desiccation · Shrinkage · Suction · Analytical modelling

Introduction

Evaporation is an essential part of the water cycle. Water evaporation is established from saturated soil surface, in contact with air. In hydrology, evaporation is collectively termed evapotranspiration. Water evaporation occurs when the soil surface is exposed to a more or less dry environment, allowing water molecules to escape and form water vapour. In geotechnical and environmental engineering, increasing attention has been paid to the coupled thermo-hydro-mechanical problems of clayey soils. This is partially due to the increased number of catastrophic landslide, induced by the degradation of soil strength triggered by humidification/desiccation cycles (Philip 1957; Or 1996; Tang et al. 2008; Trabelsi 2014). The dryness phenomenon causes a considerable damage to structures built on initially quasi-saturated soils.

On one hand, the investigation of a water retention curve and permeability as a function of cracked soil is crucial to the soil stability study and long-term risk assessment for waste disposal sites, recharge estimation for groundwater hydrogeology and petroleum engineering. Dams and clayey landfills may create shrinkage with different intensities in relation with the stress histories, initial hydraulic conditions, grain-size distributions of the used materials, permeability etc. (Trabelsi 2014, 2017; Trabelsi and Frikha 2017).

On the other hand, many hydrological and plant physiological studies require soil hydraulic property measurements at both lower and higher suctions with large samples. In this study, the soil hydraulic properties were experimentally determined, using the natural evaporation method. Then, the examined soil, containing a double porosity (cracks or secondary porosity) due to shrinkage effects, was studied. Our focus was

This article is part of the Topical Collection on *Georesources and Environmental Management*

✉ Bilel Hadrich
bilel.hadrich@enis.tn

[1] National Engineering School of Tunis, Civil Engineering laboratory, University of Tunis EL Manar, B.P. 32, 1002-Le Belvédère, Tunis, Tunisia

[2] National Engineering School of Sfax, University of Sfax, Sfax, Tunisia

[3] National Engineering School of Sfax, Unité de Biotechnologie des Algues, University of Sfax, Sfax, Tunisia

[4] Higher Institute of Technological Studies of Nabeul-ISET, Nabeul, Tunisia

on explaining how the cracks evolution, and therefore the volume change during the drying path, would result in the intrinsic permeability change.

Two principal processes govern the water flux exchange between the soil and the atmosphere. Water enters the soil surface as a liquid and goes out from the soil surface as vapour through the evaporation process. Evaporation in porous media is an important process in geotechnics and environment. In fact, many physical effects are considered, such as water and heat transfer in soil. Water flow on the soil surface, being in contact with the atmosphere, is useful to predict the soil's behaviour during the evaporation process. Our investigation here, was to describe how dry air flowing through saturated soil, can partially change its volume (shrinkage phenomenon) and its mechanical behaviour (Konrad and Ayad 1997; Mihoubi et al. 2002; Trabelsi et al. 2012).

Desiccation cracking in dried soil is a common natural phenomenon, which significantly affects the soil's mechanical and hygroscopic behaviour (Louati et al. 2016; Trabelsi and Jamei 2016). In this study, experimental desiccation tests were conducted on a clayey soil. Several aspects of the soil behaviour, mainly water evaporation and volume shrinkage, were investigated here. Engineers have traditionally used a term defined as potential evaporation (PE) to estimate water evaporation or evapotranspiration rates (Ward Wilson et al. 1994) and actual evaporation (AE) or evaporation rate (R_e) to estimate the actual evaporation in unsaturated soil.

The aim of this work is to determine the intrinsic permeability of a characterised Tunisian soil under desiccation (drying path). Six analytical models were newly proposed, to describe many direct or/and indirect relationships between those hygroscopic and mechanical behaviours and several other physical soil proprieties, such as moisture content, saturation degree, void ratio etc.

Soil properties, method and test procedure

Soil properties

Grain-size distribution curve

The soil used in this study is a clayey soil from Beja (North-West of Tunisia) retrieved from an area close to the National Tunisian Road RN 11, which was damaged after landslides which were triggered by rainfall in November 2011.

Figure 1 shows the grain-size distribution curve (GSDC) of the natural material, in which a dominant particle size of 55 μm was detected. The plasticity index (I_p) = 32%, liquid limit (ω_L) = 62%, plastic limit (ω_P) = 30%, and shrinkage limit (ω_{SL}) = 15%, have been determined in a previous work (Trabelsi 2014). Table 1 summarises the geotechnical properties of the clay, classified as high-plastic inorganic clay (CH).

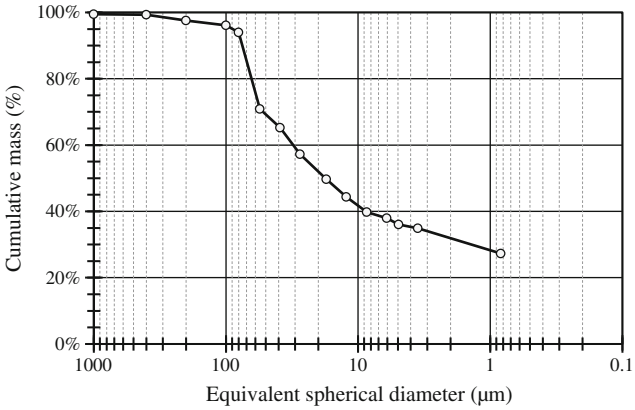

Fig. 1 Grain-size distribution curve (GSDC) of natural material

Initial drying soil water retention curve

Two techniques were used to measure the soil suction at the equilibrium state of humidity, namely the mid-range tensiometer for suctions which was lower than 100 kPa (T5x, UMS, Germany) and the Dew Point Mirror Psychrometer (WP4, Decagon Devices Inc., USA) from 100 kPa to 200 MPa. As can be seen in Fig. 2, the different techniques display consistent results. A consistent trend was obtained through tensiometer and psychrometer results.

The initial Soil Water Retention Curve (SWRC) for slurry soil prepared at 1.5 ω_L, illustrated in Fig. 2, shows the capacity of gravity water to be dried at different suctions and the water retention characteristics of the soil exposed to drying. The SWRC was determined following a drying path, under unstressed conditions and starting from remoulded state without considering the crack effect. An air-entry value of around $s_{AE} = 0.45$ MPa could be identified in Fig. 2.

The fitting of the experimental data by Van Genuchten's (1980) model (Eq. 1) was established via the least square method by minimising the difference between the experimental data and the calculated data (Fig. 2).

$$S_r = S_{res} + (S_{sat} - S_{res}) \times \left(1 + \left(\frac{P_g - P_l}{P_0}\right)^{\frac{1}{1-\lambda}}\right)^{-\lambda} \quad (1)$$

where S_r is soil saturation degree (%), $s = P_g - P_l$ is suction (MPa); P_g and P_l are gas and liquid pressure, respectively (MPa), S_{res} and S_{sat} are the residual saturation and maximum saturation degrees (%), respectively; P_0 (MPa) is a capillary pressure parameter; and λ is an empirical constant affecting the curve shape (Van Genuchten 1980).

The fitting quality was tested by two statistical coefficients: the coefficient of determination (R^2) (Eq. 2) and the root-mean-square error (RMSE) (Eq. 3). In fact, R^2 is the proportion of the sum of squares in the dependent variable

Table 1 Physical properties of the natural Beja clay

Soil properties	Value
Solid density (ρ_s)	2.70 g/cm^3
Liquid limit (ω_L)	62%
Plasticity index (I_P)	32%
Plastic limit (ω_P)	30%
Shrinkage limit (ω_{SL})	15%
Fraction of fines (< 80 μm)	97%
Clay-size fraction (< 2 μm)	18%
Water content under hygroscopic conditions (relative humidity, 50%)	4.3%
Clay minerals (qualitative DRX)	Illite, smectite
Specific surface (mercury intrusion porosimetry)	24 m^2/g

that is predictable from the independent variables. The RMSE is a frequently used measure of the differences between the values predicted by a model and the observed ones.

$$R^2 = \frac{\sum_{i=1}^{n}\left(\hat{y}_i - \overline{y}\right)^2}{\sum_{i=1}^{n}\left(y_i - \overline{y}\right)^2} \quad (2)$$

$$\mathrm{RMSE} = \sqrt{\frac{\sum_{i=1}^{n}\left(\hat{y}_i - y_i\right)^2}{n}} \quad (3)$$

where $\hat{y}_i$ and y_i: are the calculated and experimental data; $\overline{y}$: is the arithmetic mean; and n is the total number of experimental points.

The Van Genuchten model fitting quality was very good, showing a very high $R^2 = 98\%$ and a very low RMSE = 0.036. The identified parameters of the Van Genuchten model are $S_{res} = 5\%$; $S_{sat} = 98\%$; $\lambda = 0.3$; and $P_0 = 1.03$ MPa. For the studied soil, the suction of the air-entry value is around $s_{AE} = 0.45$ MPa.

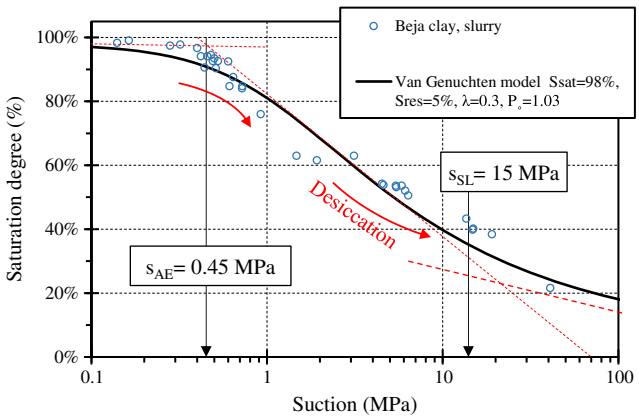

Fig. 2 Soil water retention curve (SWRC) for initial drying curve of Beja clay slurry soil

Method and test procedure

In this research, the slurry soil was sieved through 400 μm. The passing material was used in the tests at a slurry condition. The tested material was saturated with distilled water. The initial moisture content was approximately 1.5 ω_L, and it was then poured into circular glass plates with 80 mm in diameter at different heights (1, 8, 14 and 19 cm) corresponding to four specimens (E1, E2, E3 and E4). All of them were dried in the same testing climatic conditions (a relative humidity HR = 60 ± 5% and a temperature $T = 35 \pm 1$ °C). The relative humidity and temperature of the neighbouring air was measured through a hygrometer (model: ETP110). A final void ratio of $e_{min} = 0.73$ was finally achieved after air drying at an ambient relative humidity inside laboratory. To overcome this climatic condition, we used a controlled temperature climatic chamber. It was equipped with a box with water proof walls, digital cameras and a balance with an accuracy of 0.1 g, thermocouples and bulbs. The initial water content (ω_i), void ratio (e_i) and thicknesses (H_i) are given in Table 2. The grooves of the mould were intended to prevent the shrinkage during drying. It can be observed that the corresponding effect is negligible for thickness and that the shrinkage corresponds to a crack on perimeter (lateral surface).

When the slurry sedimentation started, a thin water layer appeared on the surface. This film of water was not considered in the thickness measurement; however, it was considered in the weight measurement. During drying, the specimens were weighed, which allowed the recording of water loss at varying intervals. Water content changes (ω) and water evaporation rate (R_e) (mm/day) during the drying time were then calculated. At the same measurement time, a digital camera was fixed directly above the specimens and was used to monitor the surface crack pattern evolution. Therefore, the crack heights and surfaces were determined by the images' analysis technique.

The volume change of the material was continuously monitored to correctly estimate the saturation degree during the shrinkage phenomenon. The physical properties and initial conditions are summarised in Tables 1 and 2.

Determination of intrinsic permeability via an oedometric test

To measure the permeability saturated coefficient, a suitably adapted oedometer was used in this investigation (Fig. 3). The slurry clay with water content of 1.5 ω_L was placed in a cell for 24 h. As a first step, the consolidation stress was increased gradually. After 24 h (stabilisation of deformation), the porosity and void ratios were determined, and then a hydraulic gradient of 44 (dimensionless) was applied. The hydraulic head was evaluated as a function of time through Darcy law

Table 2 Specimens initial conditions

	ω_i (%)	H_i (cm)	e_i (−)	PE (mm/days)
E1	109	1	2.97	2.85
E2	78.6	8	2.09	2.49
E3	54.8	14	1.42	3.91
E4	98.6	19	2.60	4.71

for a falling water head for an increment of time (Δt), and the intrinsic permeability (K; m^2) was determined.

Evaporation rate determination

The evaporation rate (R_e; or actual evaporation, mm/day) is defined using Eq. (4):

$$R_e = 10\frac{\Delta m}{\Delta t \times S \times \rho_w} \tag{4}$$

where: Δt: is the time interval (day); Δm: is the mass variation during the time interval (g); S: is the section of the specimen (cm^2); and ρ_w: is the water density (g/cm^3).

Results

Intrinsic permeability

The saturated permeability coefficient (K_{sat}) for most soils was considered a constant measured experimentally. This assumption is valid with sands or silts, but for clay (i.e. deformable soil), it is a current porosity evolution (ϕ) function and desiccation cycles (Rodríguez et al. 2007; Louati et al. 2016; Chaduvula et al. 2017; De Camillis et al. 2017; Mazzieri et al. 2017).

Two commonly used models were chosen from literature to fit the experimental intrinsic permeability as a porosity function: Rodríguez et al. (2007) model (Eq. 5) (this model is like that presented by Taylor 1948) and Kozeny (1927) model (Eq. 6).

$$K_{sat}(\phi) = K_0 \times exp(b \times (\phi - \phi_0)) \tag{5}$$

$$K_{sat}(\phi) = K_0 \times \frac{\phi^3 \times (1-\phi_0)^2}{\phi_0{}^3 \times (1-\phi)^2} \tag{6}$$

where b is a material parameter (soil characteristic) and K_0 is the reference intrinsic permeability corresponding to the reference porosity of ϕ_0.

The obtained fitting results are not very interesting for the two models. In fact, the corresponding R^2 of the two models do not exceed 31%. This result confirms that Rodríguez et al.'s (2007) and Kozeny's (1927) models are not suitable for the obtained experimental data. Therefore, a new Power function (Eq. 7) was proposed in this work (called model 1).

$$K_{sat}(\phi) = K_0 \times \frac{\phi^m}{(\phi_r - \phi)^n} \tag{7}$$

where ϕ_r, m, and n are the fitting parameters. ϕ_r is the porosity corresponding to the moisture content equal to the ω_L. At this moisture content, going from the liquid phase to plastic phase, permeability decreases significantly.

The identified parameters of the proposed law (model 1) (Eq. 7), which are $m = 12$, $n = 2$ and $K_0 = 7.85 \times 10^{-15}$ m^2, were determined for a porosity of $\phi_r = 0.625$. This newly established model presents a very good relationship between the intrinsic permeability and porosity in the measured range from $\phi_{min} = 0.43$ to $\phi_r = 0.625$. The calculated results from the proposed law are shown in Fig. 4a. The proposed law matches the experimental results with a higher $R^2 = 81\%$ and a lower RMSE $= 2.170 \times 10^{-15}$. Thus, the first proposed law in this work can be adopted for the experimental data, presenting the intrinsic permeability as a porosity function.

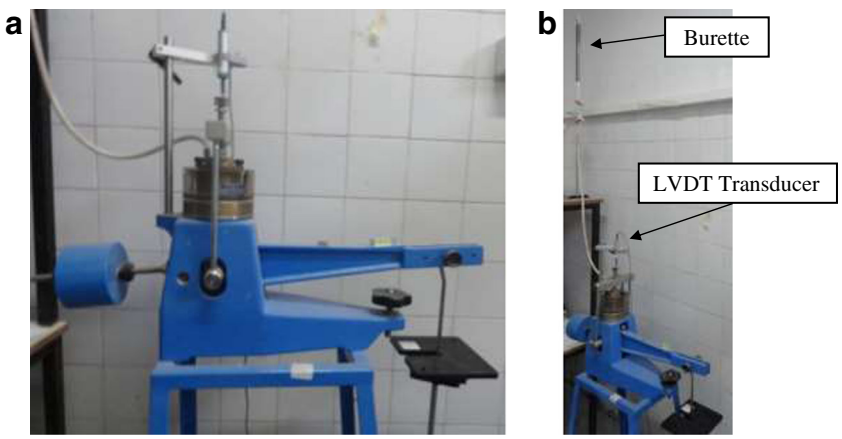

Fig. 3 Modified front loading oedometer (consolidation apparatus) with permeability attachment connected to the End Cap of the Hoek Cell (Burette 50 ml capacity and 0.1 ml div)

Figure 4b presents the variation of the intrinsic permeability and void ratio as a function of effective stress, for loading and unloading paths. The obtained results present standard profiles for both values.

Global representation of drying curve under nil external mechanical stress (desiccation)

As can be seen in Fig. 5, the global presentations of the drying curves consist of:

- The moisture content variation throughout the drying time (Fig. 5a).
- The saturation degree variation during desiccation (Fig. 5b). To determine the saturation degree, we used the image analysis technique to determine the height and the crack intensity factor (CIF). The crack volume and settlement are subtracted from the total volume. In fact, Trabelsi (2014) proves that the crack initiation and propagation is quickly established from surface to bottom. In his research, the crack depth is considered equal along the specimen depth. The mercury immersion method, usually used to determine the exact shrinkage volume, is destructive, and this is not suitable for the entire desiccation path. However, the image analysis technique was recently used by Trabelsi and Frikha (2017) for two types of soil and proved the accuracy of the results.
- The change in saturation degree as a moisture content function is presented in Fig. 5c.

Examining Fig. 5, samples E3 and E4, for example have two close thicknesses (14 and 19 cm), but they have two very different initial moisture contents ($\omega_i = 54.8$ and 98.6%, respectively). The moisture content decreases linearly, when the saturation degree is higher than 95% (phase I corresponding to the constant drying rate, when $\omega_i \geq 50\%$; Fig. 5c) and reaches the hydraulic equilibrium when the saturated degree reaches 21% (decreasing drying rate, when $\omega_i \leq 50\%$; Fig. 5c). When $\omega_i \leq 50\%$, desiccation produces a shrinkage with unsaturated porous media. This shrinkage tends to generate a radial tensile stress. When this phenomenon reaches the tensile strength, crack networks appear (Trabelsi et al. 2010; Trabelsi 2014; Latifa et al. 2015; Jommi et al. 2016). Jommi et al. (2016) proved that the tensile strength depends on depth along the desiccation path. In addition, the shrinkage phenomenon tends to decrease the specimen total volume. The sample mass is obviously constant. Then, only the void volume decreases during desiccation. So, the void ratio value decreases and affects especially the intrinsic permeability (Rodríguez et al. 2007).

Global representation of the evaporation curve under fixed climatic conditions

The evaporation rate was determined for all the experiments. The corresponding values are presented as a function of four important parameters: drying time (Fig. 6a), saturation degree (Fig. 6b), suction (Fig. 6c) and moisture content (Fig. 6d).

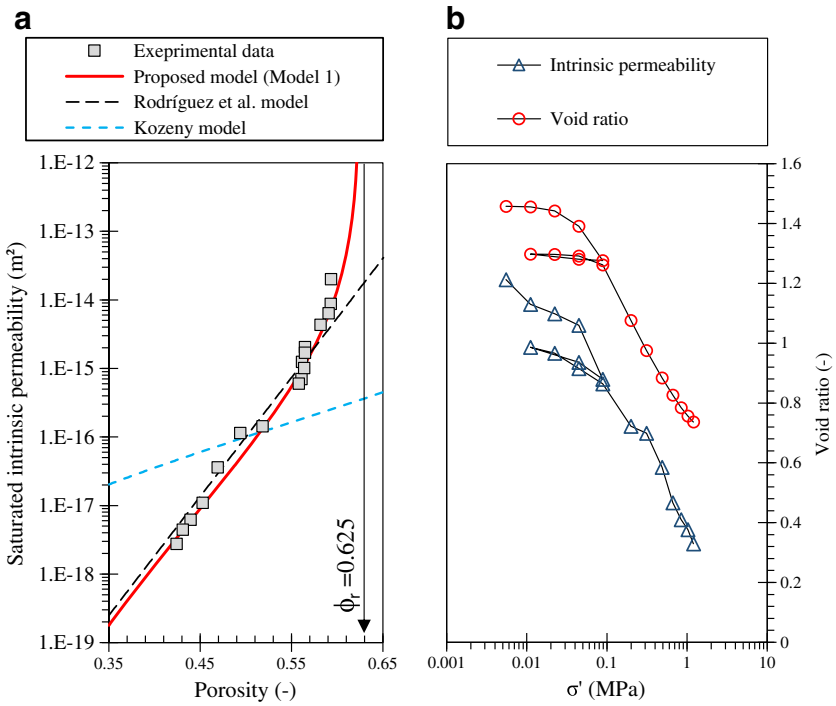

Fig. 4 Change in permeability for the slurry sample: **a** as a function of porosity and **b** as a function of the effective stress (σ')

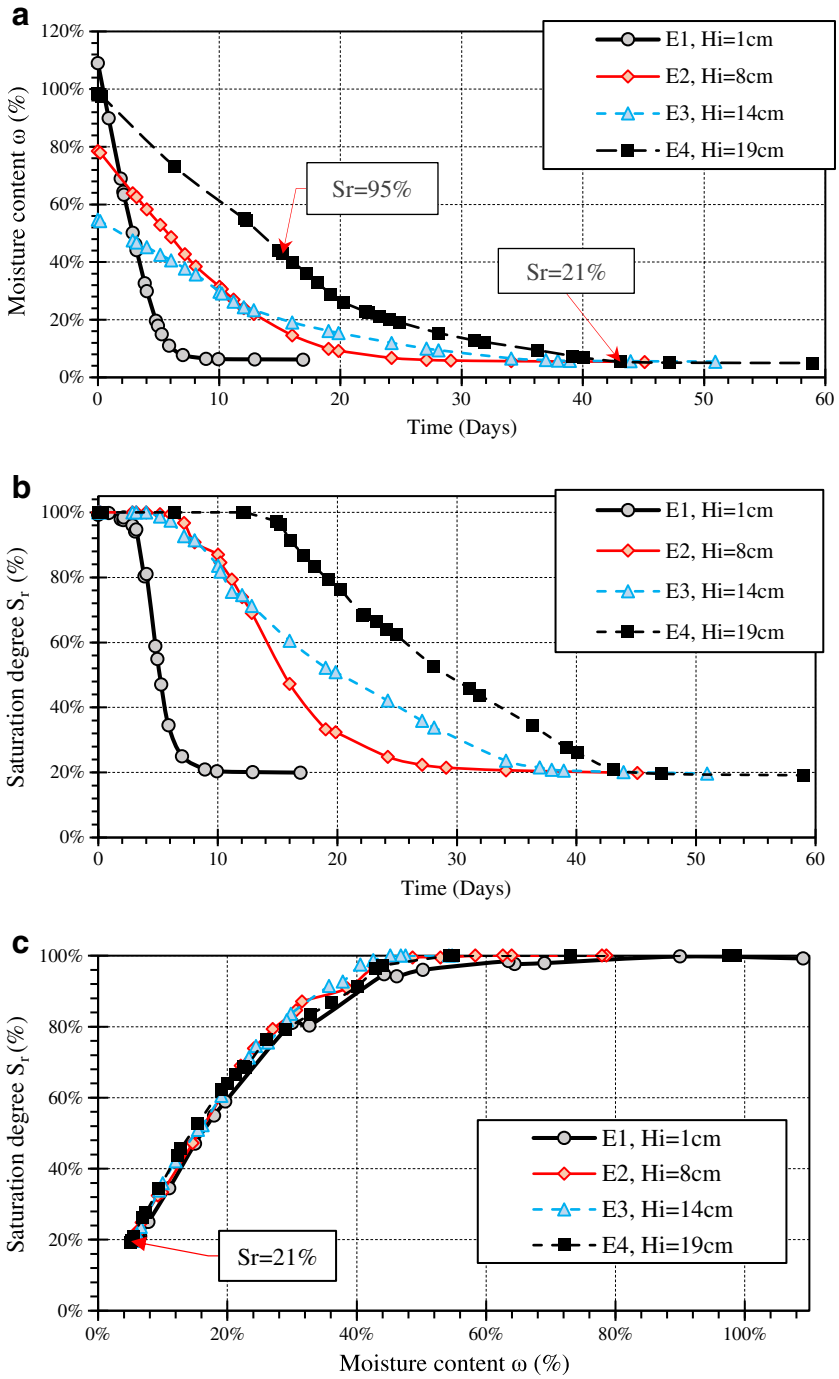

Fig. 5 Drying curves. **a** Moisture content versus time, **b** saturation degree versus time and **c** saturation degree as function of moisture content

Three stages can also be observed for all the experiments:

- The first stage is characterised by a quasi-constant evaporation (Fig. 6a–c) during the first 5 to 10 days, corresponding to a quasi-saturated soil ($95 < S_r < 100\%$) (Fig. 6b) and a moisture content less than 40% (Fig. 6d). This phase period depends on the hydraulic conductivity as well as the climatic conditions. This first stage is called the pendular stage. The increase of fluctuation in the beginning of all the experiments (in the first days), can be due to the samples' behaviour versus the experimental environment (samples adaptation). Some peaks in Fig. 6a (during the pendular regime) can be caused by the crack opening.
- In the second stage, this crack was characterised by the CIF which is presented next. The evaporation rate decreases linearly as function of saturation degree ($21 < S_r < 95\%$) (Fig. 6b). This second stage is called the funicular stage.

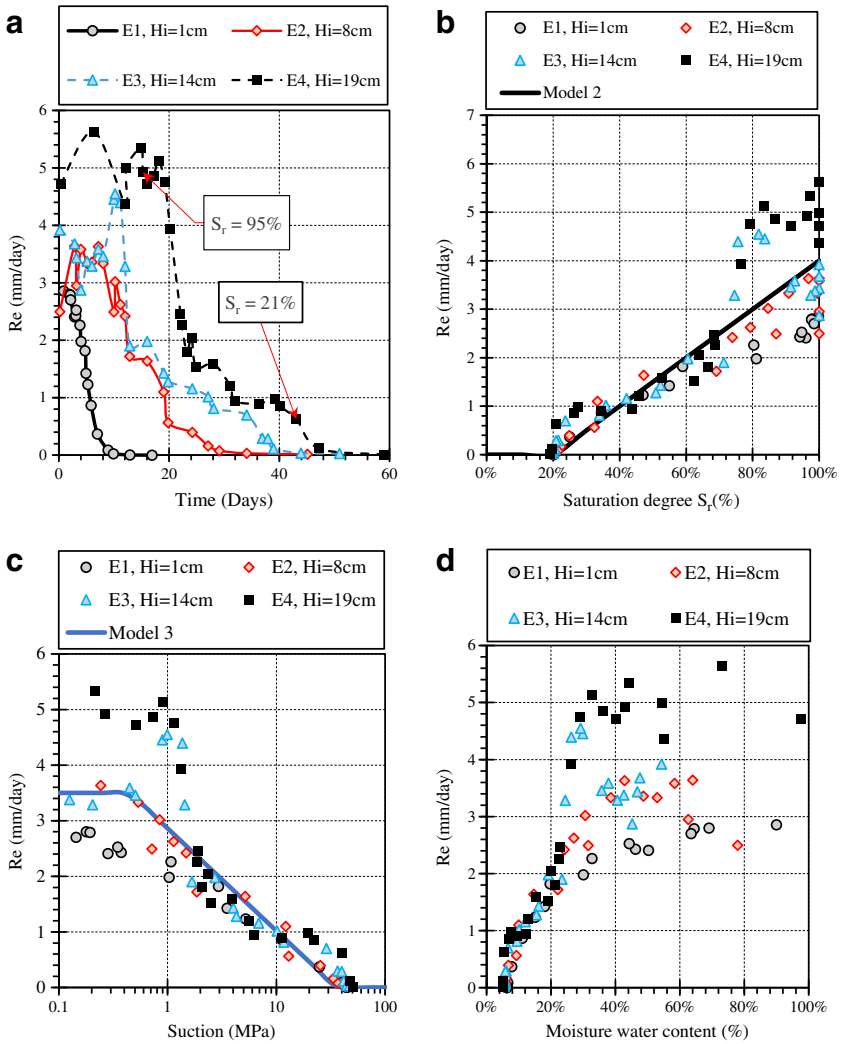

Fig. 6 Evaporation rate during desiccation process and relationship between evaporation rates versus **a** time, **b** saturation degree, **c** suction and **d** moisture water content

- The last stage is the capillary regime stage ($S_r \approx 21\%$). In this stage, the soil tends to an equilibrium.

Modelling the evaporation rate versus saturation degree and suction

S_{res} and S_{sat} are the residual saturation and maximum saturation degrees.

Figure 6b shows a linear relationship between the evaporation rates as a saturation degree function, within the range of 20–100% only. In this case, we can define a S_{res} of 20% and an initial saturation degree S_r^i of 100%. An average evaporation PE potential, for the saturated stage ($S_r^i = 100\%$), is calculated from all the experiments. A given value of around PE = 4 mm/day was chosen. PE represents the evaporation capacity of the soil under a complete saturated condition.

The proposed evaporation rate and saturation degree relationship was defined by Eq. (8) (called model 2). The corresponding result is shown in Fig. 6b:

$$R_e = PE\left(\frac{S_r - S_{res}}{S_r^i - S_{res}}\right) \tag{8}$$

The fitting quality of Model 2 was measured by the coefficient of determination R^2 equal to 77.6% and an RMSE equal to 0.750. These statistical parameters prove that Model 2 can be considered acceptable for the experiments range (Fig. 6b).

The experimental observation of soil water evaporation from the saturated state generally indicates two main phases in relation to suction (Fig. 6c). The first phase corresponds to a constant evaporation rate over time ($95 < S_r < 100\%$ and $3 < R_e < 5$), in which suction develops slowly and the soil remains in a saturated state. In the second phase, the evaporation rate decreases rapidly, and the soil suction increases significantly ($21 < S_r < 95\%$ and $1 < R_e < 3$). At the end of this phase, the

evaporation rate reaches the residual value, which depends on the soil characteristics and climatic conditions. Combining this finding with the water retention curve (Fig. 2), the relationship between the evaporation rate and the soil suction was determined. The evaporation rate was calculated based on the soil suction. The third proposed model (model 3) is defined as follows (Eq. 9):

$$R_e(s) = max\left\langle PE' - \beta\left(Ln\left(\frac{S}{S_{AE}}\right) + \left|Ln\left(\frac{S}{S_{AE}}\right)\right|\right); 0\right\rangle \quad (9)$$

where s is the suction, s_{AE} is suction of air-entry value (0.45 MPa) and β is a curve coefficient. The parameters were obtained by minimising the error between the calculated values using model 3 and the evaporation rate evolution experimental points, via the least square method. The obtained results were $\beta = 0.4$ mm/day and $PE' = R_e$ $(S_r = 90\%) =$ 3.5 mm/day. PE′ corresponds to the evaporation rate, exactly at the time corresponding to the air-entry. When s is less than s_{AE}, this quantity $\left(\mathrm{Ln}\left(\frac{S}{S_{AE}}\right) + \left|\mathrm{Ln}\left(\frac{S}{S_{AE}}\right)\right|\right)$ becomes equal to zero and then $R_e(s) = PE'$.

The fitting has a very good quality with a higher $R^2 = 83\%$ and a lower value of RMSE = 0.722.

These modelling investigation results can be considered important, since models 2 and 3 allow determining the evaporation rate value (and obviously, the corresponding drying time) for any saturation degree and/or suction determined experimentally from any sample of this soil type.

Crack network

The crack pattern characteristics were quantified using the commonly used image analysis technique (Vogel et al. 2005; Costa et al. 2008; Tang et al. 2008; Trabelsi and Jamei 2016). To this end, computer-operated digital cameras were positioned directly above the upper and lateral surfaces of each mould. These cameras were programmed to take the samples snapshots, which were automatically saved throughout the tests. Since the crack network involves segments and nodes formation (Liu et al. 2013), and aiming to quantify the cracking intensity and distribution, several parameters should be defined (Nahlawi and Kodikara 2006). In this work, the CIF evolution (calculated according to Eq. 10) was presented. The CIF was described as an indicator of surface cracking (Vogel et al. 2005; Costa et al. 2008; Tang et al. 2008; Trabelsi and Jamei 2016; Trabelsi and Frikha 2017).

$$CIF = {}^{A_c}/_{A} \quad (10)$$

with A_c as the crack area and A as the sample total area.

The calculated areas used above were determined using recorded images during drying. These images were converted to binary images, where the set of white pixels represented clayey aggregates and the black ones the crack network.

Figure 7 shows the sample E1 before (Fig. 7a) and after (Fig. 7b) the test. The image analysis was performed in two basic steps. The first involved the preparation of the image, in which the original digital image colour was processed in various stages, including conversion of the image colour (Fig. 7b) to a grey-scale image and then to a binary (black-and-white) image (Fig. 7c) by thresholding the grey-scale image (Fig. 7d). The second step consisted in analysing the processed image to obtain the parameters that characterise the crack pattern. This was achieved by performing several types of binary operations depending on the desired magnitude. The public domain program ImageJ, with plug-ins and additions, was used to carry out these operations.

The main objective of the image analysis was the study of the crack intensity factor evolution through time, for which sequences of images representing the initiation, formation and evolution of cracks during the experiment were used.

Figure 8a shows the evolution of the CIF samples during the drying time. The lower the depth is, the faster the initiation of cracks will be. In addition, the cracks start at a moisture content around $\omega = 44\%$ (Fig. 8b) and remain constant when the moisture content reaches the shrinkage limit $\omega_{SL} = 15\%$. As observed previously (Tang et al. 2010, 2011), when the actual suction is smaller than the s_{AE} (0.45 MPa) no cracks appear. This observation is still valid for E4 with an initial depth of 19 cm and an initial moisture content higher than 1.5 ω_L. However, for sample E1 corresponding to an initial depth of 1 cm and an initial moisture content also higher than 1.5 ω_L, the crack networks appear before reaching air-entry value. This can probably be induced by the friction effect. For E2 and E3, the initial moisture content is less than 1.5 ω_L and the cracks appear before reaching the air-entry value. For each sample, cracks appear when the soil saturation degree reaches 95% (Fig. 8c). The crack increases until a saturation degree of 60% and stabilises at the residual state.

Settlement and shrinkage

The volume change during shrinkage is associated with cracks and vertical strain (ε_{zz}). By determining the CIF and considering the crack thickness in depth as constant and continuing to the bottom, we can determine the crack volume (v_c.). The solid volume (v_s) was considered constant. The settlement ($h_0 \times \varepsilon_{zz}$, with h_0 is the initial high) was quantified by the image analysis technique using a lateral picture, taken automatically at the same time with a surface picture. Figure 9a presents the vertical strain (ε_{zz}) during desiccation. It can be observed that in the beginning, the water loss was accompanied by a volume change induced only by settlements, until a moisture content close to 44% corresponding to the air-entry value. The vertical strain presents two linear phases: before and after the air-entry

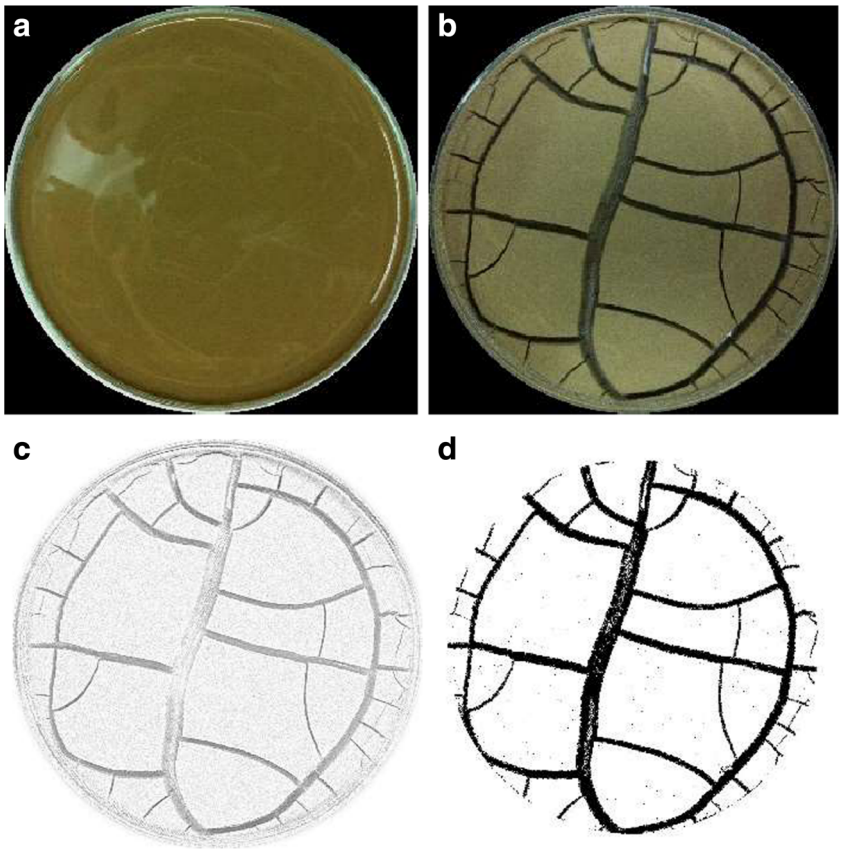

Fig. 7 Crack networks: **a** saturated soil at the beginning of test and **b** dried soil at the end of the test. **c**, **d** an example of performed image analysis technique

value (with a higher R^2 of 79–99.5% and a very low RMSE of 0.90–2.76). Indeed, in the saturated phase, the slopes of all the curves vary as a function of the ω_i and they are expressed as 1.3–0.63 ω_i. The equation was determined by the least square method. However, for the unsaturated phase, the slopes are constant and are equal to 0.25.

At a given time, the total volume associated with the soil sample is the sum of three volume components: v_s, v_p and v_c volumes. In fact, the solid volume corresponds to the solid mass (m_s) divided by the solid density (ρ_s.). The pores volume corresponds to voids in the soil mass. By quantifying the three different components of soil shrinkage, we can determine the net dry density (ρ_d.). This is one of the main advantages of the practice used in this research and previously (Sanchez et al. 2013). The advantage of quantification of the volume changes associated with each component after the crack network generation is the clay medium characterisation. The dry density variation (and the void ratio), that effectively takes place during shrinkage (Eqs. 11 and 12), is corrected by subtracting the crack volume from the void volume (Eqs. 13 and 14).

In fact, the soil mechanics classical formulas are:

$$\rho_d = \frac{m_s}{v} = \frac{m_s}{v_s + v_p + v_c} \tag{11}$$

$$e = \frac{v_v}{v_s} = \frac{v_p + v_c}{v_s} \tag{12}$$

To calculate the dry density (ρ_d) and the void ratio (e), we propose, in this work, to consider only the v_p without v_c as follows:

$$\rho_d = \frac{m_s}{v_s + v_p} \tag{13}$$

$$e = \frac{v_p}{v_s} \tag{14}$$

From Eqs. 13 and 14, the dry density can be calculated by Eq. (15):

$$\rho_d = \frac{\rho_s}{1 + e} \tag{15}$$

where $\rho_s = 2.7$ g/cm^3 is the solid density.

Figure 9b shows the change in dry density versus moisture content in the compaction diagram presented with three types of tests: the first one was applied on slurry and dried samples, the second was applied for the consolidated specimen (at the end of oedometric test) and submitted to desiccation at the same hygrothermal condition applied in the first test (main drying curve), and the third test was performed on compacted states (Standard Proctor test energy). The soil volumetric shrinkage takes place during desiccation for the first and the second tests. The third test corresponding result (Standard Proctor test), is presented in the same diagram. The dry

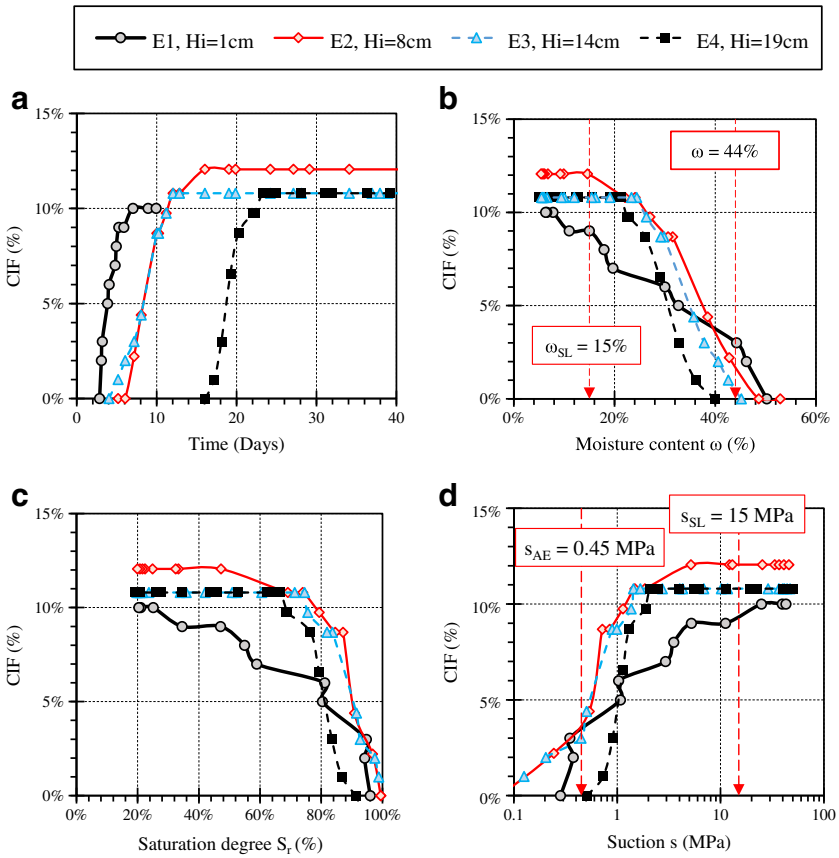

Fig. 8 Variation of CIF versus **a** time, **b** water content, **c** saturation degree and **d** suction

density increases for all samples, when the moisture content decreases from slurry ($S_r = 100\%$) to residual state ($S_r = 20\%$), under the desiccation (drying path). The modelling of this relationship was carried out with a newly proposed model 4 ('Correlation of porosity with suction and moisture') in the following section (Fig. 9b). For the proctor test, the dry density is above the desiccation path experiments for a first domain ($60 < S_r < 85\%$). Otherwise, when the soil saturation degree is lower than 60%, the dry density becomes lower than the desiccation path. Therefore, the corresponding mechanical energy has a significant influence on the first domain only. For the main drying curve, the specimens consolidated inside the oedometer cell under $\sigma' = 1$ MPa (Fig. 4b), the mechanical deformation increases the dry density a little bit. The dry density at the residual state tends approximately to the same values of the natural shrinkage curve. The main curve is always higher than the natural shrinkage and standard proctor.

To show the similarity between the two used methods (effect of suction and that of mechanical stress) within the interval 0.1 to 1 MPa, an oedometric test was performed. The oedometric curve was compared with the drying path curves in the same diagram (e, s) (Fig. 10). The results show that the experimental drying curves are close to the oedometric one (consolidation). When the oedometric test was finished, the consolidated sample was dried. The consolidate-drying variation (main drying curve; Pham et al. 2005) curve is negligible compared with the initial slurry with a nil initial stress. In the engineering application, this clay can be stabilised by consolidation under mechanical stress in the order of 1 MPa, before building. In fact, during desiccation (main drying curve), the consolidated clay has a little shrinkage.

The proctor energy increases the dry density only when saturation is in the range of 60–80%. In addition, the soil final dry density is higher than the optimum dry density (Standard Proctor). On the contrary, for the consolidated soil with a stress around 1.2 MPa, the final dry density is a little higher than the dried soil. The global representation highlights the difference in the soil shrinkage and saturation behaviour, with respect to moisture. In the (ω, e) plan (Fig. 11), the different heights of the different samples having different initial moisture contents approximately coincide with each other.

Unsaturated soil behaviour modelling

To study the behaviour of drying soil based on image analysis technique, a novel method was presented in this paper. The results presented above are used in this section to predict the intrinsic permeability variation with the respective volume change. To understand the soil drying process by modelling its behaviour, some correlations were presented.

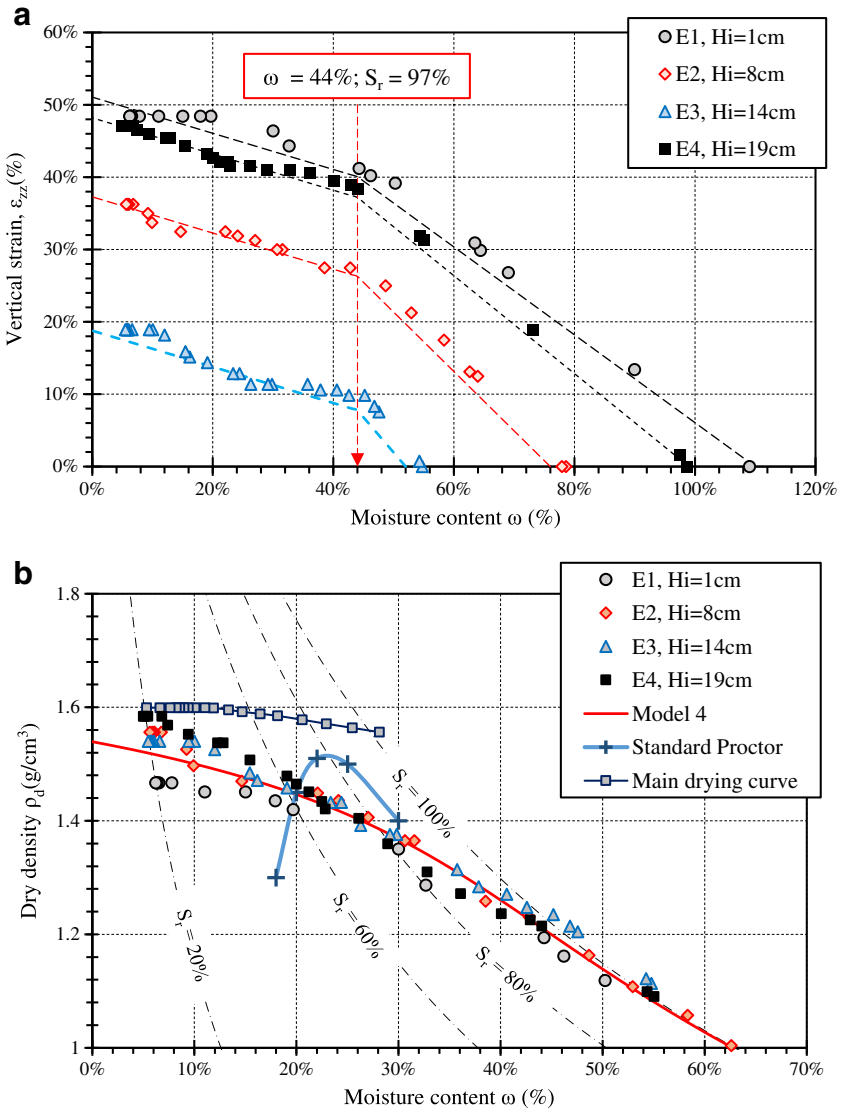

Fig. 9 The followed shrinkage paths **a** in terms of vertical strain and **b** dry density versus moisture content plotted in the compaction diagram

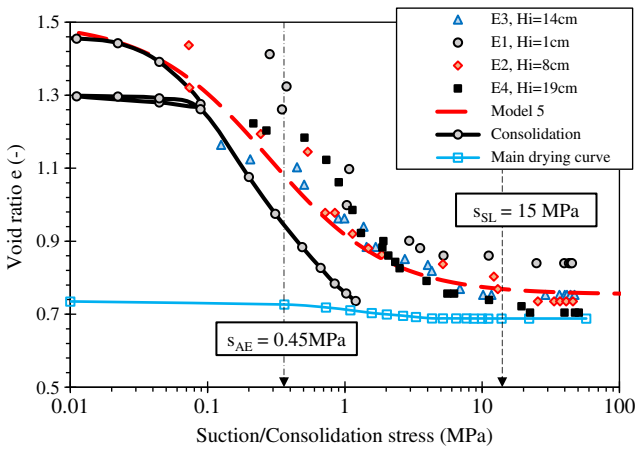

Fig. 10 Comparison between drying and oedometric curves

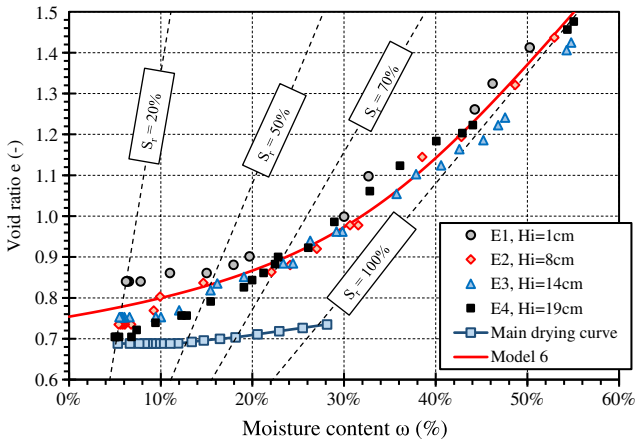

Fig. 11 The followed shrinkage paths in terms of void ratio versus water content

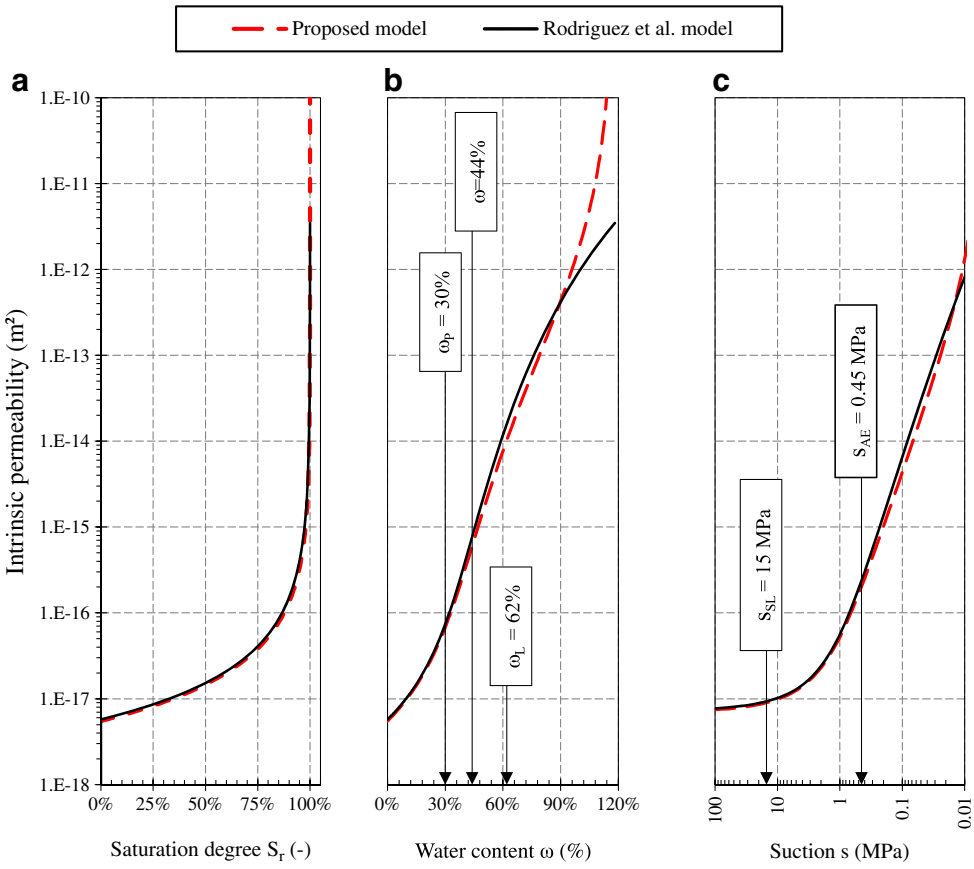

Fig. 12 The followed shrinkage paths in terms of permeability versus **a** saturation degree, **b** water content and **c** suction

Correlation of porosity with suction and moisture

To highlight the effect of soil retention properties on the drying curves in the present study, the s_{AE} and shrinkage limit suction (s_{SL}) were chosen as the basic parameters, to characterise the drying curves main properties. A correlation was established between porosity and suction variation (Model 4) (Eqs. 16–17):

$$\phi(s) = \phi_{min} + (\phi_r - \phi_{min})\left(\frac{S_{AE}}{S + S_{AE}}\right) \tag{16}$$

with $\phi_{min} = 0.43$ and $\phi_r = 0.625$ are the minimum and the maximum porosities (corresponding to the moisture content equal to the liquid limit), respectively.

The dry density (Eq. 15) and water content are directly calculated as a function of the void ratio as follows (Eq. 17):

$$\rho_d = \frac{S_r \times e(s) \times \rho_w}{\omega \times (1 + e(s))} \tag{17}$$

where ρ_w is water density (1 g/cm^3).

The void ratio was then directly calculated as follows (Eq. 18; Fig. 10, model 5):

$$e(s) = \frac{\phi(s)}{1 - \phi(s)} \tag{18}$$

Model 6 was proposed in this work to express the void ratio (e) versus saturation degree (S_r). The model expression is presented in Eq. (19) as follows:

$$S_r = 1 - \left(\frac{e_{min}}{e}\right)^n \tag{19}$$

where $e_{min} = 0.754$; $n = 7$ is a material parameter.

Model 6 presents a high fitting quality because R^2 and RMSE are equal to 96% and 4.749, respectively. The graphical result is shown in Fig. 11. Finally, the suction was calculated using SWRC and Van Genuchten's (1980) model.

Correlation of void ratio with unsaturated permeability

The intrinsic permeability is a soil characteristic that reflects the ability by which a porous medium allows fluids to pass through. The change in void ratio of the remoulded soil is used to estimate the change in its intrinsic permeability. The combination of model 1 (and obviously Rodríguez et al.'s (2007) law) and model 5 allows determining the intrinsic permeability as a suction function (Fig. 12c). By means of Eqs. 7, 16, 18 and 19, we can determine the intrinsic permeability as a saturation degree function (Fig. 12a). Finally, with Eq. (17), we found the intrinsic permeability as a moisture content function

(Fig. 12b). These curves present the unsaturated permeability variation during desiccation only for the matrix without considering the cracks effects. Cracks can increase the permeability values to up to three orders of magnitude larger than the permeability of intact clay (Drumm et al. 1997; Albrecht and Benson 2001; Nyambayo et al. 2004). These findings agree with those of Gueddouda et al. (2016). Figure 12 shows very interesting results. In fact, the modelling of the intrinsic permeability behaviour allows the possibility of its determination versus the saturation degree, water content or suction of the studied soil.

Conclusions

This paper outlines the characterisation of the soil from Béja (Tunisia). This region is highly concerned with deep or shallow landslides induced by rainfall infiltration. In general, the desiccation humidification phenomenon induces the degradation of soil characteristics. The evaporation phenomenon during desiccation was also studied. In fact, the evaporation rates present three stages. During the first stage, the soil is quasi-saturated, and the evaporation rate is quasi-constant. In the second stage, the evaporation rate and the saturation degree decrease linearly. Finally, the capillary regimes stage is reached. A linear relationship between the evaporation rates versus saturation degree was also proposed in this work. However, the evaporation rates as a suction function presented two phases, and a model was proposed to identify this characteristic. The dry density versus moisture content, characterising the shrinkage phenomenon, was also modelled.

The moisture and porosity are two factors that govern the intrinsic permeability for a deformable soil. The saturation degree is usually used for determining a relative permeability without deformation. Proposed models presented in this paper consider porosity, saturation degree, moisture content and suction for the estimation of intrinsic permeability curves for a deformable soil. The intrinsic permeability is controlled by the porosity as soil suction changes. The unsaturated permeability curves and relative permeability coefficient are significantly influenced by suction, water content and saturation degree. The experimental data proved the proposed correlations. Our future potential work will investigate the crack effect of unsaturated soil on permeability.

References

Albrecht BA, Benson CH (2001) Effect of desiccation on compacted natural clays. J Geotech Geoenviron 127(1):67–75

Chaduvula U, Viswanadham BVS, Kodikara J (2017) A study on desiccation cracking behavior of polyester fiber-reinforced expansive clay. Appl Clay Sci 142:163–172

Costa S, Kodikara J, Thusyanthan NI (2008) Study of desiccation crack evolution using image analysis. In: Toll DG, et al. (eds) Unsaturated soils: advances in geo-engineering. DOI: https://doi.org/10.13140/2114634843

De Camillis M, Di Emidio G, Bezuijen A, Flores DV, Van Stappen J, Cnudde V (2017) Effect of wet-dry cycles on polymer treated bentonite in seawater: swelling ability, hydraulic conductivity and crack analysis. Appl Clay Sci 142:52–59

Drumm E, Boles D, Wilson G (1997) Desiccation cracks result in preferential flow. Geotech News 15(2):22–25

Gueddouda MK, Goual I, Benabed B, Taibi S, Aboubekr N (2016) Hydraulic properties of dune sand–bentonite mixtures of insulation barriers for hazardous waste facilities. J Rock Mech Geotech Eng 8(4):541–550

Jommi C, Valimberti N, Tollenaar RN, Della Vecchia G, van Paassen LA (2016) Modelling desiccation cracking in a homogenous soil clay layer: comparison between different hypotheses on constitutive behaviour. In: E3S Web of Conferences, vol. 9, p. 08006. EDP Sciences

Konrad JM, Ayad R (1997) Desiccation of a sensitive clay: field experimental observations. Can Geotech J 34(6):929–942

Kozeny J (1927) Uber Kapillare Leitung des Wassersim Boden. Sitzungsber Akad Wiss Wien 136:271–306

Latifa E, Houcem T, Mehrez J, Romero E (2015) Dessication effects on clay-based engineered barriers. In: International symposium on energy geotechnics

Liu C, Tang CS, Shi B, Suo WB (2013) Automatic quantification of crack patterns by image processing. Comput Geosci 1(sur 257):77–80

Louati F, Houcem T, Jamei M (2016) Experimental and numerical investigation about permeability of clay subjected to humidification-desiccation cycles. 3ème colloque international sur les sols non saturés (UNSAT Batna 2015), At BATNA

Mihoubi D, Zagrouba F, Ben AM, Bellagi A (2002) Drying of clay. I. Material characteristics. Dry Technol 20(2):465–487

Mazzieri F, Di Emidio G, Pasqualini E (2017) Effect of wet-and-dry ageing in seawater on the swelling properties and hydraulic conductivity of two amended bentonites. Appl Clay Sci 142:40–51

Nahlawi H, Kodikara JK (2006) Laboratory experiments on desiccation cracking of thin soil layers. Geotech Geol Eng 1(sur 224):1641–1664

Nyambayo VP, Potts DM, Addenbrooke TI (2004) The influence of permeability on the stability of embankments experiencing seasonal cyclic pore water pressure changes. In: Advances in geotechnical engineering: the Skempton conference: proceedings of a three-day conference on advances in geotechnical engineering, organised by the Institution of Civil Engineers and held at the Royal Geographical Society, London, UK, 29–31 March. Thomas Telford Publishing, pp. 898–910

Or D. Wetting-induced soil structural changes: the theory of liquid phase sintering. Water Resour Res, vol. 32, n°110, p. 3041–3049, 1996

Pham HQ, Fredlund DG, Barbour SL (2005) A study of hysteresis models for soil-water characteristic curves. Can Geotech J 42(6):1548–1568

Philip J. R., Evaporation, and moisture and heat fields in the soil. J Meteorol, vol. 14, n°14, pp. 354–366, 1957

Rodríguez R., Sánchez M., Ledesma A. and Lloret A., Experimental and numerical analysis of desiccation of a mining waste. Can Geotech J, vol 44, n°16, pp. 644–658, 2007

Sanchez M, Atique A, Kim S, Romero E, Zielinski M (2013) Exploring desiccation cracks in soils using a 2D profile laser device. Acta Geotech 8(6):583–596

Tang C, Shi B, Liu C, Gao L (2010) Experimental investigation of the desiccation cracking behavior of soil layers during drying. J Mater Civ Eng 23:873–878

Tang CS, Shi B, Liu C, Suo WB, Gao L (2011) Experimental characterization of shrinkage and desiccation cracking in thin clay layer. Appl Clay Sci 52(1):69–77

Tang C, Shi B, Liu C, Zhao L, Wang B (2008) Influencing factors of geometrical structure of surface shrinkage cracks in clayey soils. Eng Geol 101:204–217

Taylor DW (1948) Fundamentals soil mechanics. Wiley, New York, pp 225–238

Trabelsi, H. Evaporation rate dependence with saturation degree. In: International congress and exhibition. Sustainable civil infrastructures: innovative infrastructure geotechnology. Springer, Cham, 2017

Trabelsi H, Frikha W (2017) Determination of shrinkage properties of clayey soils by the image analysis technique. In: International congress and exhibition. Sustainable civil infrastructures: innovative infrastructure geotechnology, pp. 51–63. Springer, Cham

Trabelsi H, Jamei M (2016) 3D desiccation crack pattern effects on UCS of clay. 3éme colloque international sur les sols non saturés unsatbatna 2015, At BATNA

Trabelsi H (2014) Etude expérimentale et numérique du comportement des argiles soumisent à des conditions de dessiccation. Thèse de doctorat ENIT, University of Tunis, Tunisie

Trabelsi H, Jamei M, Guiras H, Hatem Z, Romero E, Sebastia O (2010) Some investigations about the tensile strength and the desiccation process of unsaturated clay. EPJ Web of Conferences. France-poty: [s.n.]

Trabelsi H, Jamei M, Zenzri H, Olivella S (2012) Crack patterns in clayey soils: experiments and modeling. Int J Numer Anal Methods Geomech 36(11):1410–1433

Van Genuchten M (1980) A closed-form equation for predicting the hydraulic conductivity of unsaturated soils. Soil Sci Soc Am J 44(5): 892–898

Vogel HJ, Hoffmann H, Roth K (2005) Studies of crack dynamics in clay soil. I. Experimental methods, results, and morphological quantification. Geoderma 125:203–211

Ward Wilson G, Fredlundan D, Barbour S (1994) Coupled soil-atmosphere modelling for soil evaporation. Can Geotech J 31: 151–161